https://doi.org/10.3311/PPme.22287
Creative Commons Attribution

Periodica Polytechnica Mechanical Engineering, 67(3), pp. 197–203, 2023

New Top Land Computing Method for Spiral Bevel Gears

Miklós Gábor Várkuli[1*], Gabriella Bognár[1], József Szente[1]

[1] Institute of Machine and Product Design, Faculty of Mechanical Engineering, University of Miskolc, Egyetemváros, H-3515 Miskolc, Hungary
[*] Corresponding author, e-mail: miklos.varkuli@uni-miskolc.hu

Received: 27 March 2023, Accepted: 18 May 2023, Published online: 09 June 2023

Abstract

In this study, we present two methods for determining the top land of bevel gears. One of them that can be found in the professional literature is based on the Tredgold's virtual cylindrical gear model and, corresponding to this, deals with a limited accuracy. The alternative method developed by us is based on a mathematical modelling of the manufacturing process and involves in the computing of the top land dimensions theoretically perfect surface models.

Keywords

tooth pointing, top land, mathematical modelling, spiral bevel gears

1 Introduction

A possible gear tooth damage form is the breaking of the tooth tip. This is due to a phenomenon known as tooth pointing, a consequence of a design inaccuracy, leading to insufficient gear top land. When the load is applied to the tooth tip, the thin top land does not provide sufficient strength and the tooth tip may break off. In the case of cylindrical gears, knowing the involute geometry allows us to easily check the top land during the design procedure.

For bevel gears, especially spiral bevel gears, this task is much more complicated. The recommendations in the literature trace the investigation of bevel gears back to virtual cylindrical gears, that is, they use a method with approximate accuracy.

In this paper, we present a new, accurate method for determining the top land thickness, which is based on the mathematical modelling of the tooth surfaces. The procedure is applied to spiral bevel gears.

The mathematical modelling of tooth surfaces was based on the works of Litvin [1–3]. Tooth surface models can be used in many areas of design, such as

- tooth contact analysis and loaded tooth contact analysis [4–9];
- measuring on a coordinate measuring machine [10–12];
- finite element analysis [13–16];
- the design of non-machined (forged, molded, 3D printed) gears [17].

In their previous works, the authors used mathematical modelling of tooth surfaces for finite element analysis [18], and to determine the contact ratio [19] for spiral bevel gears.

2 Calculation of the top land according to AGMA 929-A06

AGMA 929-A06 [20] contains guidelines for calculating the top land of bevel gears. The publication is not a standard, but a technical guideline, which recommends the presented calculation method as a supplement to the geometric calculations set in the standard [21]. The method is generally accepted and used in practice.

The method is based on the Tredgold approximation which transform a bevel gear pair into a corresponding virtual cylindrical gear pair [22]. In this way, the otherwise extremely complicated problem is traced back to the examination of cylindrical gears, for which there are known and relatively simple relationships for calculating the top land.

AGMA 929-A06 [20] examines the top land along the tooth length in three normal planes:

- in the middle of the tooth,
- at the outer end of the tooth, and
- at the inner end of the tooth.

To perform the calculations, the geometric data of the bevel gear must be known. Among them, the following are required to determine the top land.

Cite this article as: Várkuli, M. G., Bognár, G., Szente, J. "New Top Land Computing Method for Spiral Bevel Gears", Periodica Polytechnica Mechanical Engineering, 67(3), pp. 197–203, 2023. https://doi.org/10.3311/PPme.22287

Pitch diameter (d_e), pitch angle (δ), outer cone distance (R_e), mean cone distance (R_m), inner cone distance (R_i), outer addendum (h_{ae}), mean addendum (h_{am}), inner addendum (h_{ai}), mean dedendum (h_{fm}), mean transverse pitch (p_m), pressure angle (α_n), cutter radius (r_c) cutter point width (P_w) which is one half of the difference between the inside and outside point diameters of an alternate blade cutter, mean spiral angle (β_m), outer spiral angle (β_e), inner spiral angle (β_i), outer slot width on mating gear (W_{el}), inner slot width on mating gear (W_{il}), outer dedendum on mating gear (h_{fel}), inner dedendum on mating gear (h_{fil}), normal blacklash at outer tooth end (B).

2.1 Tredgold's approximation

Tredgold's approximation using for spiral bevel gears is shown in Fig. 1.

Tredgold's approximation in original form was developed for straight bevel gears having involute tooth profile. The approximation means the bevel gear is substituted an equivalent spur gear. This relation is extended to spiral bevel and hypoid gears by AGMA 929-A06 [20]. Pitch surface curvature in the direction perpendicular to the gear tooth spiral defines an equivalent spur gear having involute profile.

The transverse plane is perpendicular to the elements of pitch cone in an arbitrary point *P*. The normal plane is perpendicular to both the tooth spiral and the pitch plane in the same point. The principal curvatures of the pitch cone in point *P* are:

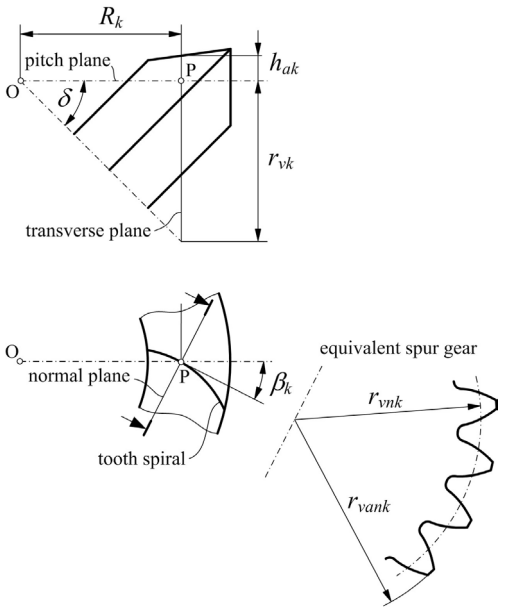

Fig. 1 Tredgold's approximation

$$\chi_1 = \frac{1}{r_{vk}} = \frac{1}{R_k \tan\delta}, \text{ and } \chi_2 = 0. \tag{1}$$

The curvature of pitch cone in the normal plane is:

$$\chi_n = \chi_1 \cos^2\beta_k + \chi_2 \sin^2\beta_k = \frac{\cos^2\beta_k}{R_k \tan\delta}. \tag{2}$$

The pitch circle radius of the equivalent spur gear equals the radius of curvature of pitch cone in the normal plane:

$$r_{vnk} = \frac{1}{\chi_n} = \frac{R_k \tan\delta}{\cos^2\beta_k}. \tag{3}$$

The equivalent spur gear has the following dimensions:

$$\text{Base circle radius}: \quad r_{vbnk} = r_{vnk}\cos\alpha_n, \tag{4}$$

$$\text{Tip circle radius}: \quad r_{vank} = r_{vnk} + h_{ak}. \tag{5}$$

2.2 Determination of top land

The top land dimension of bevel gear equals the tooth thickness of equivalent spur gear measured on tip circle. Using dimensions from Fig. 1, the top land can be calculated as follows:

$$s_{vank} = \left(\frac{s_{vnk}}{2r_{vnk}} + \text{inv}\alpha_n - \text{inv}\alpha_{vank}\right)2r_{vank}, \tag{6}$$

where:

- s_{vnk} is the tooth thickness at pitch circle,
- r_{vnk} is the pitch circle radius,
- α_n is the pressure angle,
- α_{vank} is the pressure angle at tip circle.

The pressure angle at tip circle is defined as:

$$\alpha_{vank} = \arccos\frac{r_{vbnk}}{r_{vank}}, \tag{7}$$

In Eq. (6), inv is the involute function, the interpretation of which is for any angle x:

$$\text{inv}x = \tan x - x.$$

AGMA 929-A06 [20] defines the top land in three positions: at the two tooth ends and in the middle of the tooth. By changing the subscript to $k = e$, $k = m$, $k = i$ in Eqs. (1)–(7) of the general solution the relationships valid for the investigated sections are obtained.

The individual characteristics in the examined sections are as follows:

1. Pitch circle radii:

$$r_{vne} = \frac{R_e \tan\delta}{\cos^2 \beta_e}, \tag{8}$$

$$r_{vnm} = \frac{R_m \tan\delta}{\cos^2 \beta_m}, \tag{9}$$

$$r_{vni} = \frac{R_i \tan\delta}{\cos^2 \beta_i}. \tag{10}$$

2. Base circle radii:

$$r_{vbne} = r_{vne} \cos\alpha_n, \tag{11}$$

$$r_{vbnm} = r_{vnm} \cos\alpha_n, \tag{12}$$

$$r_{vbni} = r_{vni} \cos\alpha_n, \tag{13}$$

3. Tip circle radii:

$$r_{vane} = r_{vne} + h_{ae}, \tag{14}$$

$$r_{vanm} = r_{vnm} + h_{am}, \tag{15}$$

$$r_{vani} = r_{vni} + h_{ai}. \tag{16}$$

4. Pressure angles at tip circle:

$$\alpha_{vane} = \arccos\frac{r_{vbne}}{r_{vane}}, \tag{17}$$

$$\alpha_{vanm} = \arccos\frac{r_{vbnm}}{r_{vanm}}, \tag{18}$$

$$\alpha_{vani} = \arccos\frac{r_{vbni}}{r_{vani}}, \tag{19}$$

5. Tooth thicknesses on pitch circle [20]:

$$s_{vne} = W_{e1} + 2h_{fe1}\tan\alpha_n - \frac{B}{\cos\alpha_n}, \tag{20}$$

$$s_{vnm} = p_m \cos\beta_m - P_w - 2h_{fm}\tan\alpha_n, \tag{21}$$

$$s_{vni} = W_{i1} + 2h_{fi1}\tan\alpha_n - \frac{R_i \cos\beta_i}{R_e \cos\beta_e}\frac{B}{\cos\alpha_n}. \tag{22}$$

6. Tooth thicknesses on tip circle:

$$s_{vane} = \left(\frac{s_{vne}}{2r_{vne}} + \text{inv}\alpha_n - \text{inv}\alpha_{vane}\right)2r_{vane}, \tag{23}$$

$$s_{vanm} = \left(\frac{s_{vnm}}{2r_{vnm}} + \text{inv}\alpha_n - \text{inv}\alpha_{vanm}\right)2r_{vanm}, \tag{24}$$

$$s_{vani} = \left(\frac{s_{vni}}{2r_{vni}} + \text{inv}\alpha_n - \text{inv}\alpha_{vani}\right)2r_{vani}. \tag{25}$$

3 Calculation of top land by mathematical model of tooth surfaces

For the mathematical modelling of the tooth surfaces of the bevel gear, the following data or preliminary calculations are required:

- geometrical data of the bevel gear;
- cutter dimensions: cutter radius, blade angle, the relative position of the blades working on the two tooth sides;
- machine setting data: the relative position of the tool and the workpiece on the machine tool;
- movement conditions: the coordinated movement of the tool and the workpiece during production.

3.1 Creation of tooth surface models

A precise mathematical description of the tooth surfaces is possible with knowledge of the production and its precise modelling. Fig. 2 shows a Gleason-type manufacturing

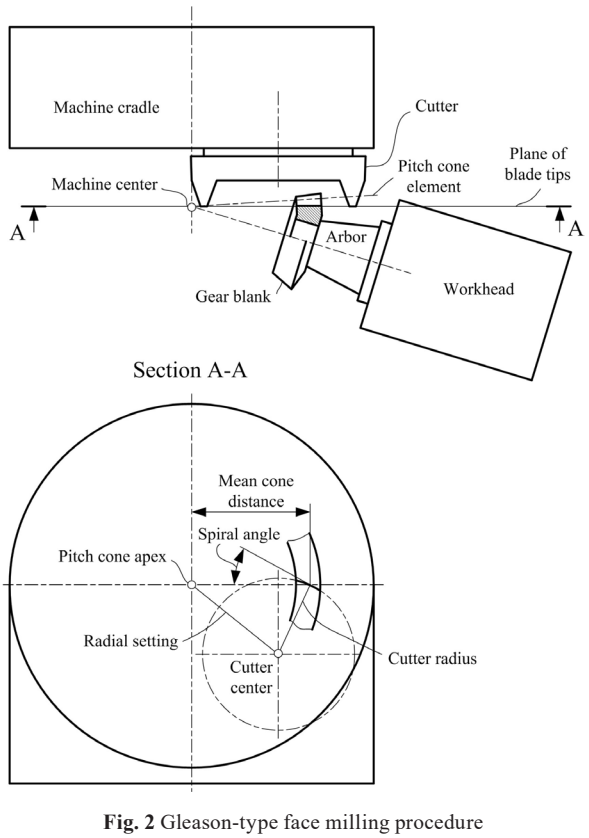

Fig. 2 Gleason-type face milling procedure

method for spiral bevel gears. The chipping results from the rotating movement of the cutter head. This movement is independent of other motions that determine the shape of the tooth surface. During rotation, the cutting edges of the tool produce a surface of rotation, which is called generating surface. The position vector of the generating surface can be described with two parameters:

$$\boldsymbol{r}_{cj}\left(s_j,\theta_j\right). \tag{26}$$

Since the generating surface is different for the convex and the concave tooth side, the parameters can also be different, i.e., $j = d$ for the convex and $j = h$ for the concave tooth side.

The generating surface results in a family of surfaces in the relative movement, which in the coordinate system fixed to the workpiece, with its origin located at the apex of the pitch cone, is Eq. (27):

$$\boldsymbol{r}_j\left(s_j,\theta_j,\psi_j\right)=\boldsymbol{M}_j\left(\psi_j\right)\boldsymbol{r}_{cj}\left(s_j,\theta_j\right). \tag{27}$$

Here, $\boldsymbol{M}_j$ is the matrix of the transformation, ψ_j is the motion parameter.

To produce the tooth surface, we need to find a relationship between the three parameters of the family of surfaces. One possible way to do this is to obtain partial derivatives and solve Eq. (28):

$$\left(\frac{\partial \boldsymbol{r}_j}{\partial s_j}\times\frac{\partial \boldsymbol{r}_j}{\partial \theta_j}\right)\times\frac{\partial \boldsymbol{r}_j}{\partial \psi_j}=f\left(s_j,\theta_j,\psi_j\right)=0. \tag{28}$$

Here, the first term in brackets on the left side is the normal at the instantaneous point of contact, the second term is the quantity proportional to the relative velocity at the same point. Equation (28) is the equation of meshing.

Using the parameter relation generated from the solution of Eq. (28), the equation of the tooth surface of bevel gear is available in Eq. (29):

$$\boldsymbol{r}_j\left(\theta_j,\psi_j\right)=\boldsymbol{r}_j\left(s_j\left(\theta_j,\psi_j\right),\theta_j,\psi_j\right). \tag{29}$$

According to our comment regarding Eqs. (26) and (29) is valid for both tooth sides with the limitation that the individual parameters must be taken into account according to the current tooth side, i.e., $j = d$ for the convex and $j = h$ for the concave tooth flank.

3.2 Selection of the points to be investigated

We will mark three points on the face cone of the bevel gear, as in Section 2: on the two tooth ends and in the middle of the tooth. The location of the examined points is given by the radial (U) and axial (V) coordinates measured from the apex of the pitch cone of bevel gear.

Fig. 3 shows an arbitrary F point on the face cone element. The coordinates of this point are:

$$U_k = R_k\sin\delta + h_{ak}\cos\delta, \tag{30}$$

$$V_k = R_k\cos\delta - h_{ak}\sin\delta. \tag{31}$$

Coordinates of the investigated points are obtained from general equations using $k = e$, $k = m$ and $k = i$ subscripts. That is:

$$U_e = R_e\sin\delta + h_{ae}\cos\delta, \tag{32}$$

$$V_e = R_e\cos\delta - h_{ae}\sin\delta, \tag{33}$$

$$U_m = R_m\sin\delta + h_{am}\cos\delta, \tag{34}$$

$$V_m = R_m\cos\delta - h_{am}\sin\delta, \tag{35}$$

$$U_i = R_i\sin\delta + h_{ai}\cos\delta, \tag{36}$$

$$V_i = R_i\cos\delta - h_{ai}\sin\delta. \tag{37}$$

In Eqs. (34)–(37) the following connections are applied:

$$R_m = R_e - \frac{b}{2}, \tag{38}$$

$$R_i = R_e - b, \tag{39}$$

$$h_{am} = h_{ae} - \frac{b}{2}\tan\theta_a, \tag{40}$$

$$h_{ai} = h_{ae} - b\tan\theta_a. \tag{41}$$

3.3 Parameters and coordinates of the selected points on the tooth surfaces

Equation (29) position vector given with the coordinates is the following:

$$\boldsymbol{r}_j\left(\theta_j,\psi_j\right)=\begin{bmatrix}x_j\left(\theta_j,\psi_j\right)\\ y_j\left(\theta_j,\psi_j\right)\\ z_j\left(\theta_j,\psi_j\right)\end{bmatrix}. \tag{42}$$

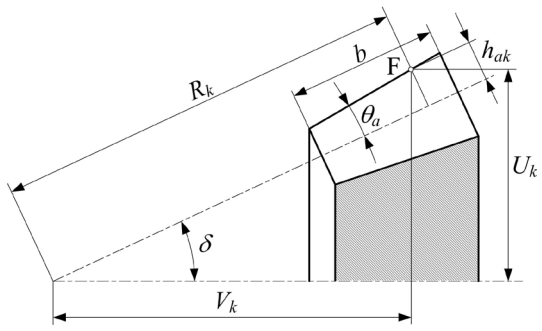

Fig 3 Arbitrary point on face cone element

The location of any point on the tooth surface can be determined by solving the following system (Eq. (43)) of non-linear equations:

$$\left[x_j\left(\theta_j,\psi_j\right)\right]^2+\left[y_j\left(\theta_j,\psi_j\right)\right]^2=U_k^2,\ z_j\left(\theta_j,\psi_j\right)=V_k. \quad (43)$$

The parameters θ_j and ψ_j are available as a solution to equation system (Eq. (43)), so the coordinates of the point on the tooth surface can be determined.

The parts in Eq. (44) display six systems of equations due to the two tooth sides ($j = d$, h) and three points per tooth side ($k = e$, m, i). Denote the solutions by θ_{de}, θ_{dm}, θ_{di}, θ_{he}, θ_{hm}, θ_{hi} and ψ_{de}, ψ_{dm}, ψ_{di}, ψ_{he}, ψ_{hm}, ψ_{hi}. With these the coordinates of the six points:

$$\begin{aligned}
&x_{de}\left(\theta_{de},\psi_{de}\right),\ y_{de}\left(\theta_{de},\psi_{de}\right),\ z_{de}\left(\theta_{de},\psi_{de}\right),\\
&x_{dm}\left(\theta_{dm},\psi_{dm}\right),\ y_{dm}\left(\theta_{dm},\psi_{dm}\right),\ z_{dm}\left(\theta_{dm},\psi_{dm}\right),\\
&x_{di}\left(\theta_{di},\psi_{di}\right),\ y_{di}\left(\theta_{di},\psi_{di}\right),\ z_{di}\left(\theta_{di},\psi_{di}\right),\\
&x_{he}\left(\theta_{he},\psi_{he}\right),\ y_{he}\left(\theta_{he},\psi_{he}\right),\ z_{he}\left(\theta_{he},\psi_{he}\right),\\
&x_{hm}\left(\theta_{hm},\psi_{hm}\right),\ y_{hm}\left(\theta_{hm},\psi_{hm}\right),\ z_{hm}\left(\theta_{hm},\psi_{hm}\right),\\
&x_{hi}\left(\theta_{hi},\psi_{hi}\right),\ y_{hi}\left(\theta_{hi},\psi_{hi}\right),\ z_{hi}\left(\theta_{hi},\psi_{hi}\right).
\end{aligned} \quad (44)$$

In a more concise form:

$$x_{jk}\left(\theta_{jk},\psi_{jk}\right),\ y_{jk}\left(\theta_{jk},\psi_{jk}\right),\ z_{jk}\left(\theta_{jk},\psi_{jk}\right). \quad (45)$$

3.4 Calculation of the top land

Top land can be determined in the transverse plane by Eq. (46):

$$s_{ak}=U_k\left(\frac{2\pi}{N}-\left|\phi_{dk}-\phi_{hk}\right|\right), \quad (46)$$

where the angles ϕ_{dk} and ϕ_{hk} give the location of the points on the two sides of the tooth in the transverse plane.

$$\phi_{dk}=\arctan\frac{y_{dk}}{x_{dk}}, \quad (47)$$

and:

$$\phi_{hk}=\arctan\frac{y_{hk}}{x_{hk}}. \quad (48)$$

The normal top lands are given by the spiral angles:

$$s_{ank}=s_{ak}\cos\beta_k. \quad (49)$$

4 An application example

For the practical application of the methods presented in Sections 2 and 3, we worked out a numerical example. The investigated bevel gear is a spiral bevel gear having circular arc profile along tooth length, whose geometrical data is given in Table 1.

Additional data not included in Table 1, but necessary for the calculations, were determined based on [21]. The calculation was made with three cutter radii, at three characteristic points of the bevel gear using both methods. The cutters have Gleason standard dimensions: 4.5 in (114.3 mm), 8 in (203.2 mm) and 400 mm.

The results of the calculations performed using the two methods are summarized in Table 2 and Fig. 4.

5 Summary and conclusions

When designing the gears, care must be taken to avoid tooth pointing. Tooth pointing is checked by examining the top land. There are empirical recommendations for the minimum amount of top land, usually in proportion to the module. In the case of bevel gears, the most sensitive place for tooth pointing is the inner tooth end. In this study, we presented two methods for determining the top

Table 1 Dimensions of investigated bevel gear

Designation	Notation	Data
Number of teeth	N	30
Outer transverse module (mm)	m_{te}	4.791
Face width (mm)	b	40
Pressure angle (°)	α_n	20
Mean spiral angle (°)	β_m	30
Outer cone distance (mm)	R_e	235.01
Mean cone distance (mm)	R_m	215.01
Pitch diameter (mm)	d_e	143.73
Outer addendum (mm)	h_{ae}	3.69
Outer dedendum (mm)	h_{fe}	5.16
Cutter radius (mm)	r_c	114.3
		203.2
		400
Cutter point width (mm)	P_w	2.286
Pitch angle (°)	δ	17.8
Face angle (°)	δ_a	17.9667
Root angle (°)	δ_f	17.6333
Addendum angle (°)	θ_q	0.1667
Normal backlash at outer tooth end (mm)	B	0.15
Hand of spiral		Left
Outer slot width on mating gear (mm)	W_{el}	2.54
Inner slot width on mating gear (mm)	W_{il}	2.54
Outer dedendum on mating gear (mm)	h_{fel}	4.83
Inner dedendum on mating gear (mm)	h_{fil}	4.714

Table 2 Calculation results

	r_c = 4.5 in		r_c = 8 in		r_c = 400 mm	
	AGMA	Model	AGMA	Model	AGMA	Model
Outer	3.049	2.88	3.025	3.686	3.012	4.121
Middle	3.049	3.086	3.049	3.086	3.049	3.086
Inner	2.958	2.788	2.993	2.344	3.017	2.005

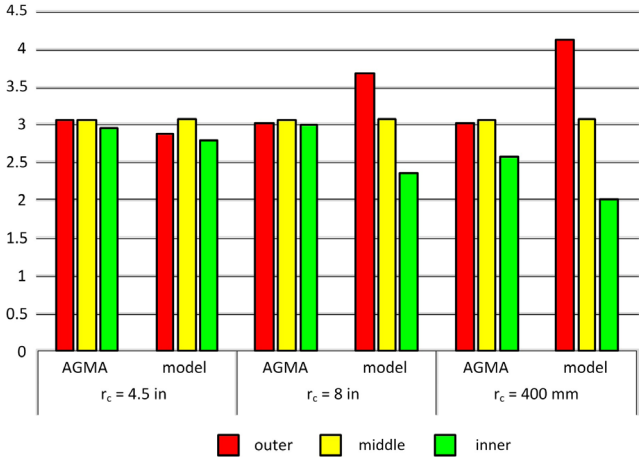

Fig. 4 Change of top land according to the cutter radius and investigated position

land of bevel gears. One of the methods known from the literature, based on virtual cylindrical gears, is a solution with approximate accuracy. The other method, developed by us, is based on a mathematical description of the production, uses theoretically accurate tooth surface models, accordingly the calculation of the top land is also possible with high accuracy.

Based on Section 2, it can be established that the AGMA calculation does not take into account the production method. From the production data, it only uses the two geometric characteristics of the cutter head (cutter radius, point width), partly through the tooth spiral angles.

The Gleason firm has developed a variety of manufacturing methods for spiral bevel gears with circular arc tooth orientation. They are generated or non-generated. Some of them without claim to completeness: single side, spread-blade, fixed setting, Unitool, VersaCut, completing. These methods have different cutters, different machine settings and different generating motions. The tooth surfaces of a bevel gear with a given geometry will be different depending on the manufacturing process. Accordingly, the shape and size of the top land will be different.

Based on Table 2 and Fig. 4, the following conclusions can be drawn from the calculation example:

- The AGMA 929-A06 [20] calculation gave an almost constant top land value for all three cutter radii and in all three examined positions. The difference between the largest and smallest value is within 0.1 mm.
- The calculation based on the tooth surface model shows a clear pattern for the two larger cutter radii: the top land is largest at the outer tooth end and decreases inwards. The change is stronger with a larger cutter radius. At the smallest cutter radius, the calculation does not follow the previous pattern. The maximum value occurs in the middle of the tooth, which is almost identical to the AGMA 929-A06 [20] result.
- Since bm does not depend on the cutter radius, the top land in the middle of the tooth is the same in all three cases. These values show a difference of only 0.037 mm for the two calculation methods.

The tests showed that the AGMA 929-A06 [20] method provides a good approximation for the calculation of the top land in the middle of the tooth, but significant errors can also occur at the ends of the teeth. The latter is a function of the cutter head size and the machine settings data.

References

[1] Litvin., F. L. "Theory of Gearing", NASA, Washington, DC, USA, Rep. 88-C-035, 1989. [online] Available at: https://ntrs.nasa.gov/api/citations/19900010277/downloads/19900010277.pdf [Accessed: 26 March 2023]

[2] Litvin., F. L. "Gear Geometry and Applied Theory", Prentice Hall, Englewood Cliffs, NJ, USA, 1994. ISBN 0132110954

[3] Litvin, F. L., Fuentes, A. "Gear Geometry and Applied Theory", Cambridge University Press, 2004. ISBN 9780511547126 https://doi.org/10.1017/CBO9780511547126

[4] Gleason Works "Understanding Tooth Contact Analysis", Gleason Machine Division SD., Rochester, NY, USA, Rep. 3139B, 1981.

[5] Fan, Q. "Enhanced Algorithms of Contact Simulation for Hypoid Gear Drives Produced by Face-Milling and Face-Hobbing Processes", Journal of Mechanical Design, 129(1), pp. 31–37, 2007. https://doi.org/10.1115/1.2359475

[6] Krenzer, T. J. "Tooth Contact Analysis of Spiral Bevel and Hypoid Gears Under Load", SAE International, USA, SAE Technical Paper 810688, 1981. https://doi.org/10.4271/810688

[7] Fan, Q., Wilcox, L. "New Developments in Tooth Contact Analysis (TCA) and Loaded TCA for Spiral Bevel and Hypoid Gear Drives", Gear Technology, 24(3), pp. 26–35, 2007. [online] Available at: https://www.geartechnology.com/ext/resources/issues/0507x/fan.pdf [Accessed: 26 March 2023]

[8] Simon, V. V. "Loaded tooth contact analysis and stresses in spiral bevel gears", In: ASME 2009 International Design Engineering Technical Conferences and Computers and Information in Engineering Conference, San Diego, CA, USA, 2009, pp. 271–279. ISBN 978-0-7918-4903-3 https://doi.org/10.1115/DETC2009-86164

[9] Vivet, M., Mundo, D., Tamarozzi, T., Desmet, W. "An analytical model for accurate and numerically efficient tooth contact analysis under load, applied to face-milled spiral bevel gears", Mechanism and Machine Theory, 130, pp. 137–156, 2018. https://doi.org/10.1016/j.mechmachtheory.2018.08.016

[10] Chambers, R., Brown, R. "Coordinate Measurement of Bevel Gear Teeth", SAE International, USA, SAE Technical Paper 871645, 1987. https://doi.org/10.4271/871645

[11] McVea, W. R., Mellis, D. W. "Spiral Bevel Tooth Topography Control Using CMM Equipment", SAE International, USA, SAE Technical Paper 911757, 1991. https://doi.org/10.4271/911757

[12] Litvin, F. L., Kuan, C., Wang, J. C., Handschuh, R. F., Masseth, J., Maruyama, N. "Minimization of Deviations of Gear Real Tooth Surfaces Determined by Coordinate Measurements", Journal of Mechanical Design, 115(4), pp. 995–1001, 1993. https://doi.org/10.1115/1.2919298

[13] Handschuh, R. F., Litvin, F. L. "How to Determine Spiral Bevel Gear Tooth Geometry for Finite Element Analysis", NASA Technical Memorandum, Washington, DC, USA, Rep. 91-C-018, 1991. [online] Available at: https://ntrs.nasa.gov/api/citations/19910021223/downloads/19910021223.pdf [Accessed: 26 March 2023]

[14] Bibel, G. D., Handschuh, R. "Meshing of a Spiral Bevel Gear Set With 3-D Finite Element Analysis", NASA Technical Memorandum, Washington, DC, USA, Rep. ARL-TR-1224. [online] Available at: https://ntrs.nasa.gov/api/citations/19970001473/downloads/19970001473.pdf [Accessed: 26 March 2023]

[15] Simon, V. "FEM Stress Analysis in Hypoid Gears", Mechanism and Machine Theory, 35(9), pp. 1197–1220, 2000. https://doi.org/10.1016/S0094-114X(99)00071-3

[16] Das, A. "Finite Element Stress Analysis of Spiral Bevel Gear", International Journal of Engineering and Technology, 9(2), pp. 616–627, 2017. https://doi.org/10.21817/ijet/2017/v9i2/170902091

[17] Fuentes-Aznar, A., Gonzalez-Perez, I., Pasapula, H. K. "Computerized Design of Straight Bevel Gears with Optimized Profiles for Forging, Molding, or 3D Printing", [pdf] Thermal Processing, 2016. Available at: https://thermalprocessing.com/wp-content/uploads/2017/201703/0317-Forging.pdf [Accessed: 26 March 2023]

[18] Várkuli, M. G., Bognár, G. V., Szente, J. "Kúpkerék Fogasfelületek Matematikai Modellezése Végeselemes Vizsgálathoz" (Mathematical Model of Spiral Bevel Gears for Finite Element Analysis), Gép, 73(3-4), pp. 98–103, 2022. (in Hungarian)

[19] Várkuli, M. G., Bognár, G. V., Szente, J. "Contact Ratio of Spiral Bevel Gears", In: Jármai, K., Cservenák, Á. (eds.) Vehicle and Automotive Engineering 4. VAE 2022. Lecture Notes in Mechanical Engineering, Springer, 2022, pp. 103–110. ISBN 978-3-031-15210-8 https://doi.org/10.1007/978-3-031-15211-5_9

[20] American Gear Manufacturers Association "AGMA 929-A06 Calculation of Bevel Gear Top Land and Guidance on Cutter Edge Radius", American Gear Manufacturers Association, USA, 2006.

[21] American Gear Manufacturers Association "ANSI/AGMA 2005-D03 Design Manual for Bevel Gears", American Gear Manufacturers Association, USA, 2006.

[22] ISO "ISO 10300-1:2014 Calculation of Load Capacity of Bevel Gears - Part 1: Introduction and General Influence Factors", International Organization for Standardization, Geneva, Switzerland, 2014.